



**HAL**  
open science

## Squeeze film effect for the design of an ultrasonic tactile plate

Mélanide Biet, Frédéric Giraud, Betty Lemaire-Semail

► **To cite this version:**

Mélanide Biet, Frédéric Giraud, Betty Lemaire-Semail. Squeeze film effect for the design of an ultrasonic tactile plate. *IEEE Transactions on Ultrasonics, Ferroelectrics and Frequency Control*, 2007, 54 (12), pp.2678 - 2688. 10.1109/TUFFC.2007.596 . hal-01110742

**HAL Id: hal-01110742**

**<https://hal.science/hal-01110742>**

Submitted on 28 Jan 2015

**HAL** is a multi-disciplinary open access archive for the deposit and dissemination of scientific research documents, whether they are published or not. The documents may come from teaching and research institutions in France or abroad, or from public or private research centers.

L'archive ouverte pluridisciplinaire **HAL**, est destinée au dépôt et à la diffusion de documents scientifiques de niveau recherche, publiés ou non, émanant des établissements d'enseignement et de recherche français ou étrangers, des laboratoires publics ou privés.

# Squeeze Film Effect for the Design of an Ultrasonic Tactile Plate

Mélanie Biet, Frédéric Giraud and Betty Lemaire-Semail, *Member, IEEE*

**Abstract**—Most of tactile displays currently built rely on pin based arrays. Yet, to simulate finely textured surfaces, this kind of tactile device is not always appropriate. In this paper, we identify the squeeze film phenomenon and we use it to design an ultrasonic tactile plate. The plate is actuated by piezoelectric ceramics and ultrasonic vibrations produced in this way generate the squeeze film effect. This enables us to simulate variable friction on the surface of the plate. Thus, to identify the squeeze film phenomenon, the study considers the case where the finger with a planar bottom surface and with epidermal ridges is placed on a rapidly vibrating plate. The overpressure is calculated and the result enables us to assess the relative coefficient of friction as a function of the vibration amplitude of the plate. Based on this principle, from both analytic and FE method studies, and given ergonomic and stimulation (squeeze film) requirements, we show that it is possible to suggest a design of a tactile plate. This gives rise to a comparison with experimental results.

## I. INTRODUCTION

WE experience everyday shapes and textures through small and big skin distortions, changes in boundary temperatures, as well as localized and distributed vibrations at the skin surface in order to explore and feel our environment. However, Human-computer interaction technology rarely relied on touch to close the communication loop for the information transfer from the computer to the user. In fact, despite the huge number of devices produced with various manufacturing and actuation technologies [1], most of the tactile displays built to this day fail to efficiently deform the skin and to be practical at the same time. For instance, in order to create discrete representations of a texture or a small shape, pin based arrays are widespread [2]. But, within the framework of the e-commerce for example, which consists in feeling a material via the internet, this kind of tactile device is not appropriate to simulate finely textured surfaces because miniaturization and technical integration problems are still to be solved. Inevitably, miniaturization will reach its limits and pin arrays technology will also impose technological and cost restraints. Another possibility for simulating finely textured surfaces is the use of the squeeze film effect principle. It has been shown that a beam excited by ultrasonic vibration can give rise to smooth or braking feeling according to the amplitude of vibration [3]. Moreover, the feeling of roughness can be generated by imposing low frequency periodic signal over the ultrasonic vibration. We have experienced this on the stator of an ultrasonic wave motor by controlling the wave's space period variation [4]. As a result, the squeeze force is also modulated and allows us to simulate several shapes of ridges at contact area. This technology is especially relevant to get more complex spatial properties with a lower number of actuators.

Nevertheless, before designing a tactile plate able to simulate this kind of sensations, it is required to better identify what happens on the contact area between a vibrating surface and a finger. In this study, it seems relevant to take into account the fingerprint undulations for the calculation of the overpressure created between the two surfaces. This is carried out in the second part of the paper. Besides, this overpressure enables us to find the relative coefficient of friction as a function of the vibration amplitude of the acoustic wave. We obtain in this way a criterion for the design of the tactile plate.

This plate (Fig. 1) can bend by means of PZT piezo-ceramics glued on one of the two surfaces. The monomorph built up in this manner is the subject of analytical and numerical studies (part III). Design of the tactile plate based on theoretical analysis and experimental evaluation is then discussed in the fourth part.

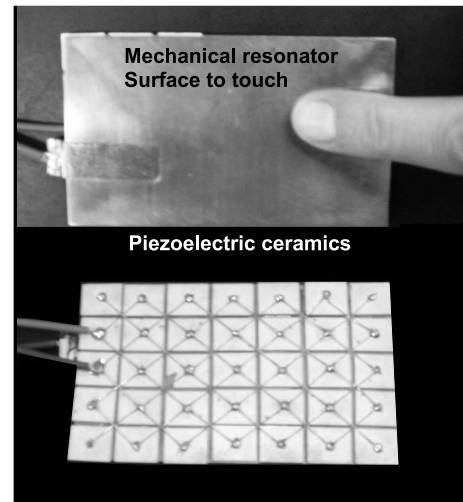


Fig. 1. Complete view of the actuator: below side with a piezo-ceramics matrix and above side which is the surface to touch

## II. SQUEEZE FILM EFFECT BETWEEN A VIBRATING SURFACE AND A FINGER

The goal of this section is to compute the overpressure force occurring because of the squeeze effect. Then it will be possible to find the conditions under which this force leads to a variation of the friction coefficient of the surface. In this section, the geometric properties of the fingerprints (or epidermal ridges) are taken into account. Effectively, we can not suppose that the undulations of the fingerprints are negligible relatively to the roughness of the vibrating plate (few micrometers) since the height ( $2h_e$ ) and pitch ( $L$ ) of the

epidermal ridge are around  $100 \mu\text{m}$  and  $350 \mu\text{m}$ , respectively [5] (Fig.2).

### A. Squeeze film model

In this subsection, we are describing the squeeze effect [6]. Indeed, we consider the gas film created between the fingertip and a planar vibrating object. We are going to rely on a study developed in [7], but taking into account the fingerprints. We regard the tip of the finger as an undulated surface while the planar plate is assumed to oscillate sinusoidally in a vertical direction (Fig.2).

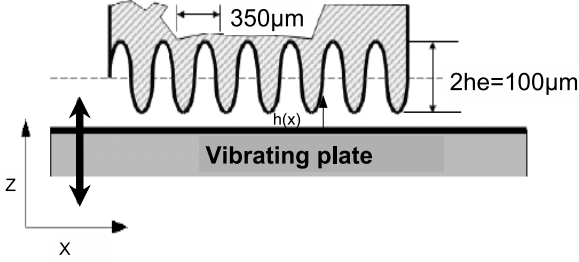


Fig. 2. Approximate profile of a fingertip when the epidermal ridges are taken into account.

The film thickness,  $h$ , is the sum of the gap created when the finger skin cannot follow the ultrasonic vibration of the plate at all, which equals the amplitude of oscillation,  $h_{vib}$ , plus the surface unevenness (roughness),  $h_r$ .  $h$  also considers the amplitude of the undulation of the fingerprint,  $h_e$ . Therefore, the thickness of the film is given by [3]:

$$h(x, t) = (h_{vib} + h_r)[1 + \cos(\omega_0 t)] + h_e[1 + \cos(\frac{2\pi}{L}x)] \quad (1)$$

In which the vibrating frequency of the plate is given by  $\omega_0$ . If we normalize  $h$ , the normalized airgap can be written with non dimensional parameters as

$$H = 1 + \epsilon \cos(T) + \delta \cos(kX) \quad (2)$$

with  $h_0 = h_{vib} + h_r$ , the non-dimensional parameters are

$$H = \frac{h}{h_0 + h_e}, \quad X = \frac{x}{l_0}, \quad T = \omega_0 t,$$

$$\epsilon = \frac{h_0}{h_0 + h_e}, \quad \delta = \frac{h_e}{h_0 + h_e}, \quad k = \frac{2\pi l_0}{L}$$

where the length in contact with the fingertip is  $l_0$ .

We make the following assumptions [7]; 1) The fluid behavior is governed by laminar viscous flow, 2) The fluid is a compressible perfect gas, 3) The inertia effect of the flow is negligible, 4) The relative lateral motion is equal to zero. Under those conditions, the one-dimensional Navier-stock equation is obtained. This equation associated with continuity and ideal gas equations allows us to find the governing Reynolds equation in the non-dimensional form:

$$\nabla(H^3 P^{1/n} \cdot \nabla(P)) = \sigma \frac{\partial(P^{1/n} H)}{\partial T} \quad (3)$$

In which  $n$  is a polytropic constant and where

$$P = \frac{p}{p_0}, \quad \sigma = \frac{12\eta\omega_0 l_0}{p_0(h_0 + h_e)^2} \quad (4)$$

$p$ ,  $p_0$  and  $\eta$  represent the pressure in the gap, the surrounding gas pressure and the dynamic viscosity of the fluid respectively. The squeeze number is given by  $\sigma$ , which represents a measurement of the fluid compressibility in the gap. At low squeeze numbers, the fluid is nearly incompressible, while at high squeeze numbers, the fluid is trapped in the gap and acts like a spring.

We further assume that the squeezed film is isothermal ( $n=1$ ). The latter assumption is reasonable since the gas film is very thin and of low heat capacity when compared with that of the vibrating surfaces. Then, to simplify the time derivation term, we substitute  $PH$  by  $\Psi$ . For steady state conditions, the integration with respect to one period yields to [7]

$$\nabla[\frac{1}{2}\bar{H}\nabla(\Psi_\infty^2) - \Psi_\infty^2 \nabla(\bar{H})] = 0 \quad (5)$$

where  $\Psi_\infty$  denotes the  $\Psi$  inside the airgap when  $\sigma \rightarrow \infty$  and  $\bar{H}$  is the mean normalized film thickness given by

$$\bar{H} = 1 + \delta \cos(kX) \quad (6)$$

It may be noticed that the analytical solution is accurate as far as  $\sigma$  is assumed at a very large value. On the contrary, a low value of  $\sigma$  would imply a much more complex solution.

### B. Approximate analytical solution

The equation 5 gives us the relationship between the normalized film thickness and the normalized pressure for a fluid behavior close to a spring. The solution of (5) is given by (Appendix A) [7]:

$$\Psi_\infty^2 = K_1[1 + \delta \cos(kX)]^2 \quad (7)$$

In which  $K_1$  is a constant.

The boundary conditions with respect to  $\Psi_\infty^2(X)$ , noted down as  $\Psi_{\infty B}$  are

$$\Psi_{\infty B}^2(-\frac{1}{2}) = \Psi_{\infty B}^2(\frac{1}{2}) = K_1[1 + \delta \cos(\frac{k}{2})]^2 \quad (8)$$

In which  $\frac{1}{2}$  is the normalized value of  $\frac{l_0}{2}$ .

By replacing  $K_1$  by its expression in (7), we obtain:

$$\Psi_\infty = \Psi_{\infty B}(\frac{1}{2}) \frac{|1 + \delta \cos(kX)|}{|1 + \delta \cos(\frac{k}{2})|} \quad (9)$$

Furthermore, in order to find  $\Psi_{\infty B}$ , we will focus our attention on the boundary region. Considering that  $p_0$  is constant in time and that  $\Psi_{\infty B}$  equals  $\Psi_\infty$  when the boundary region meets the interior of the airgap, we obtain [7]:

$$\begin{aligned} \Psi_{\infty B}^2(\frac{1}{2}) &= p_0^2 \frac{\int_T^{T+2\pi} H_B^3 dT}{\int_T^{T+2\pi} H_B dT} \\ &= p_0^2 \frac{\int_T^{T+2\pi} [1 + \epsilon \cos(T) + \delta \cos(\frac{k}{2})]^3 dT}{\int_T^{T+2\pi} [1 + \epsilon \cos(T) + \delta \cos(\frac{k}{2})] dT} \\ &= p_0^2 [1 + \delta \cos(\frac{k}{2})]^2 \left[ 1 + \frac{3}{2} \frac{\epsilon^2}{[1 + \delta \cos(\frac{k}{2})]^2} \right] \end{aligned} \quad (10)$$

By replacing  $\Psi_{\infty B}$  by its expression in (9), we obtain:

$$P_{\infty} = \frac{\Psi_{\infty}}{H} = \frac{(1 + \delta \cos(kX)) \sqrt{(1 + \delta \cos(\frac{k}{2}))^2 + \frac{3}{2}\epsilon^2}}{(1 + \delta \cos(\frac{k}{2}))(1 + \epsilon \cos(T) + \delta \cos(kX))} \quad (11)$$

Remember that  $P_{\infty}$  is the normalized pressure inside the airgap for an infinite value of the squeeze number  $\sigma$ . With  $\Omega$  as a variable position on the airgap surface, the dimensionless time average squeeze force  $F_s$  per unit length at steady state can be expressed by

$$F_s = \int \int_{\Omega} (P_{\infty} - 1) d\Omega = \frac{1}{2\pi} \int_0^{2\pi} \left( \int_{-\frac{1}{2}}^{\frac{1}{2}} (P_{\infty} - 1) dX \right) dT \quad (12)$$

Then, the mean squeeze pressure is expressed by

$$\overline{P_{\infty}} = p_0 \frac{(1 + \delta \cos(kX)) \sqrt{(1 + \delta \cos(\frac{k}{2}))^2 + \frac{3}{2}\epsilon^2}}{(1 + \delta \cos(\frac{k}{2})) \sqrt{(1 + \delta \cos(kX))^2 - \epsilon^2}} \quad (13)$$

### C. Results of the model

First of all, let us remind you that in order to predetermine analytically the over-pressure on the fingertip, we have to satisfy the following condition :  $\sigma \rightarrow \infty$ . However, we assume in practice that the squeeze force (Eq.12) depends almost entirely on the amplitude of vibration when the squeeze number is larger than 10. Therefore, we calculate the squeeze number  $\sigma$  as shown in (4), with the parameters of Table I as a function of the frequency of the oscillation for a given amplitude  $h_{vib}$ .

Considering the most unfavorable case, i.e. the smallest slope of the straight line representing  $\sigma = f(\omega_0)$  (a surface state,  $h_r$ , of  $1.6 \mu m$  and a vibration amplitude,  $h_{vib}$ , of  $3 \mu m$ ), the results (Fig. 3) show a first criterion on the frequency ( $f > 25$  kHz) which enables us to use the equation (5).

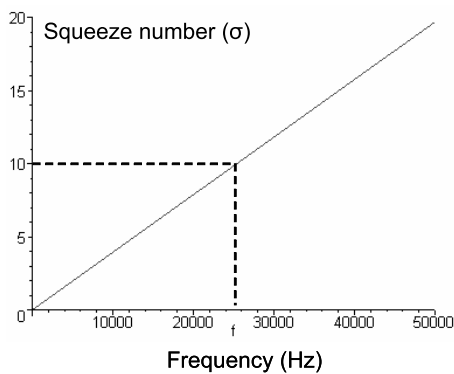


Fig. 3. Squeeze number as a function of the vibration frequency of the plate for  $h_r = 1.6 \mu m$  and  $h_{vib} = 3 \mu m$ .

Using the parameters shown in Table.I, we can compute the pressure profile along the airgap using (Eq.11). According to the previous results, the frequency of the oscillation is set to 40 kHz so as to be higher than 25 kHz.

TABLE I  
LIST OF PARAMETERS

Amplitude of the fingerprint	$h_e$	50 [ $\mu m$ ]
Period of the fingerprint	$L$	350 [ $\mu m$ ]
Average roughness of the plate	$h_r$	0.2 - 0.4 - 0.6 - 0.8 1 - 1.2 - 1.4 - 1.6 [ $\mu m$ ]
Length in contact	$l_0$	1 [cm]
Force applied by the fingertip	$F_f$	0.3 $\rightarrow$ 0.7 [N]
Dynamic viscosity of air (at 20°C)	$\eta$	$1.85 \cdot 10^{-5}$ [Pa.s]
Atmospheric pressure	$p_0$	0.1 [MPa]

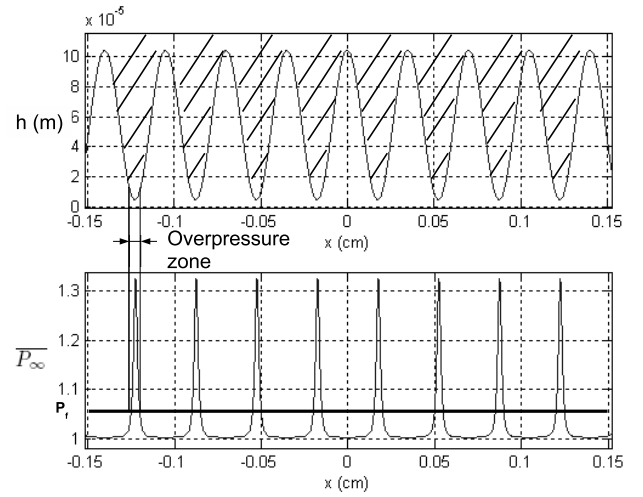


Fig. 4. Thickness of the film at a given time and spatial profile of the mean time pressure under the finger ( $h_r = 1.6 \mu m$ ,  $h_{vib} = 3 \mu m$ )

On the upper part of figure 4, the finger at contact is modeled as a sinusoid with an amplitude of  $50 \mu m$  in order to take into account the fingerprints. The interval from the zero depicts mean roughness plus the vibration amplitude of the vibrating plate itself. The curve below shows the evolution of the pressure temporal mean as a function of the position on X-axis. In this figure 4, pressure peaks are localized where the finger-skin is as close as possible to the vibrating plate, i.e. at the fingerprint ridges, whereas at the fingerprint grooves, pressure is not far from the atmospheric pressure. The pressure  $P_f$  is the mean finger pressure that it is used during an exploration task.

$$P_f = F_f / l_0^2 \quad (14)$$

where  $F_f$  denotes the normal contact force applied by a person exploring the surface. For its value, we choose 0.5 N as a mean normal contact force according to [3] [8].

We can notice from Fig. 4 that there are some zones of the fingerprint where the squeeze pressure is superior to the finger pressure. Those zones are not in contact with the vibrating plate.

Moreover, when the squeeze force occurs, we can express the relative coefficient of friction,  $\frac{\mu'}{\mu}$  in terms of (Eq.15).

$$\frac{\mu'}{\mu} = 1 - \frac{(P_{\infty} - 1)}{P_f} \quad (15)$$

Physically, and following the assumptions previously defined, this equation means a weakening of the friction coefficient for a given surface when the squeeze force occurs.

To illustrate the friction coefficient variations, we can compute  $\frac{\mu'}{\mu}$  for 8 cases of surface roughness (Table.I). The results are given in Fig.5.

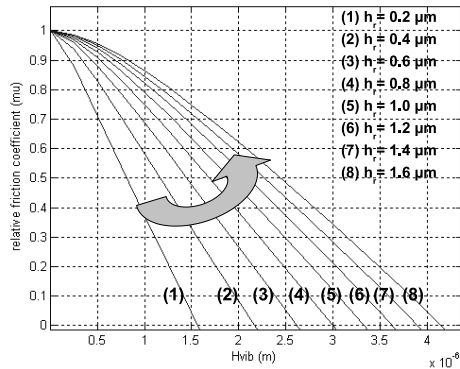


Fig. 5. The relative coefficient of friction as a function of the amplitude of vibration for  $F_f = 0.5N$  and for the 8 values of  $h_r$  (Table I)

We can easily calculate the relative friction coefficient, taking into account the fingerprints. However, our results are more pessimistic than those of Watanabe [3]. In fact, for an average roughness of a few micrometers (which is realistic from a technological point of view), a vibration amplitude of the plate higher than  $4\mu\text{m}$  would be necessary to reach a zero relative friction coefficient instead of only  $1\mu\text{m}$  found in [3]. Indeed, this is due to the consideration of the fingerprint in our study. Hence, by lubrication effect (squeeze film effect), we can succeed in changing the sensation by exploiting the friction coefficient between the finger and the plate as it was qualitatively checked in [9].

We have to notice that the relative coefficient of friction is strongly dependent on the force applied by the user ( $F_f$ ), thus the results of (Fig.5) have to be considered with care.

#### D. Guidelines for the design

Thanks to the results of (Fig.5), it is possible to foresee the vibration amplitude required to levitate the fingertip, i.e. the amplitude for which the relative coefficient of friction is annihilated. Nevertheless, the goal of our tactile device is not to induce the finger levitation. All we want to do is to decrease the friction coefficient between the surface and the finger in a significant way in order to make the user feel the difference of perception. Therefore, this analysis gives us an indication for the design of the plate. For instance, an amplitude of vibration of  $1.5\mu\text{m}$  with a carefully prepared surface ( $h_r = 0.6\mu\text{m}$ ) would be enough for the user to feel the difference of perception (half of the relative friction coefficient).

### III. DESIGN OF THE TACTILE PLATE

According to the previous study, we know the range of vibration amplitude we have to impose on the plate in order

to obtain a squeeze film effect. Now, we have to find the dimensions of the composite plate (monomorph) in order to fulfil ergonomic, amplitude and frequency requirements. To achieve this goal, we have chosen to generate ultrasonic vibrations in a plate by gluing piezoceramics on it. Thus, we are going to use the ultrasonic standing wave in this plate. It may be noticed that the motion of the surface points are no more uniform in that case. Nevertheless, we make the assumption that the overpressure will still exist. The results will be checked experimentally.

For the analytical deflection study, the simple structure considered is the half-wavelength portion of a heterogeneous beam with a rectangular section. This study enables us to determine the deflection of the beam as a function of geometrical parameters. Then, a calculation of the resonant frequency is also made as a function of geometrical parameters. Results of both the deflection and the frequency enable us to give boundaries of the numerical study. The numerical study is carried out using computation software by finite elements and allows us to justify some of the assumptions of the model.

#### A. Requirements for the design - An ergonomic workspace

The compatibility of our tactile device with the user's movement does not have to exclusively deserve the mechanisms of stimulation. It also has to offer perspectives on tangible interaction with computer-generated surfaces for example. Therefore, the definition of the ergonomic workspace plays an important role for the use of such devices. For finely textured surfaces, it is recommended to "allow the freedom of active exploration" [10]. For that purpose, the biggest exploration surface needs to be considered for the design of the tactile plate. There is no exact dimension of exploration surface in literature, but it is known, according to the observations of Klatzky and Lederman, that typically the finger quickly rubs back and forth along a small, homogeneous area of the surface, and that interior surfaces are explored rather than edges [11]. Moreover, useful information in measurements of movement amplitudes are reported in [12]. In his experiment, this author collects the position and normal force exerted by the fingertip while volunteers are actively exploring finely textured surfaces. The values for the movement amplitude along the X and Y directions are 97.27mm and 84.38mm. The mean and the biggest rectangular areas that are touched measure respectively  $28.18\text{cm}^2$  and  $128.37\text{cm}^2$ .

#### B. Analytical study

The analytical study is realized following two steps. At the first step, we begin with an analysis of the static deflection of the plate due to piezoelectric excitation. We examine a half-wavelength portion of the plate,  $\lambda/2$ , modeled as a simply-supported beam as illustrated in (Fig.6). After determining the static deflection of the plate; the deflection magnitude at resonance can be calculated by multiplying the static value by a dynamic amplification factor. At the second step, we calculate the resonant frequency as a function of the half-wavelength for a given width.

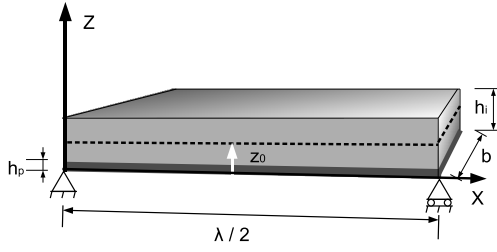


Fig. 6. A half-wavelength section of the monomorph is modeled as a simply-supported beam

1) *Determination of the static deflection:* The considered monomorph (Fig.6) consists of a layer of piezoelectric ceramic, thickness  $h_p$ , and of a layer of passive material (Copper Beryllium, for example), here called mechanical resonator, thickness  $h_i$ . Ceramic and substrate are stuck together. The working assumption retained is that this assembly is perfect, which amounts to consider that there is no thickness of adhesive and that the strains are continuous on the substrate-piezoelectric ceramic interface. The beam's length is  $\lambda/2$  and its width is  $b$ .

First of all, the displacement vector in the cartesian frame is described according to Bernoulli-Euler theory [13]

$$U = \begin{pmatrix} u \\ v \\ w \end{pmatrix} = \begin{pmatrix} (z_0 - z) \frac{\delta w}{\delta x} \\ (z_0 - z) \frac{\delta w}{\delta y} \\ w(x, y, t) \end{pmatrix} \quad (16)$$

With  $w(x, y, t)$  the displacement along the  $z$  axis, and  $z_0$  the neutral plan ordinate, which distinguishes the compression and the stretching zones into the plate.

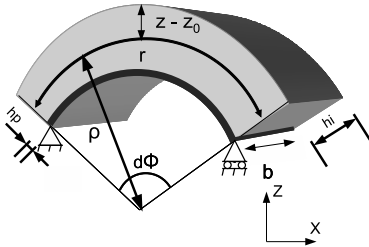


Fig. 7. Small part of the half-wavelength beam which bends by contraction of piezoceramics.

The radius of curvature,  $\rho$ , due to bending moments caused by contraction of the piezoceramic, can be determined from the resulting stresses and strains in the composite beam (Fig.7). The plate is not vibrating with a planar movement but bends. In fact, it is easier to realize bending distortion than planar distortion.

To carry out this modeling, we suppose that we are in the case of small deflections, so that all the lines which are parallel with the neutral line,  $r$ , have the same radius of curvature [14].

$$\frac{d\Phi}{r} \simeq \frac{d\Phi}{x} = \frac{1}{\rho} = \frac{d^2 w}{dx^2} \quad (17)$$

In which  $d\phi$  is the small angle between the extreme lengths of the small beam (Fig.7). The radius of curvature,  $\rho$ , due to

bending moments caused by contraction of the piezoceramic, can be determined from the resulting stresses and strains in the composite beam (Fig. 7).

If  $z_0$  denotes the neutral line ordinate and  $z - z_0$  the distance between a deformed line and the neutral line, the strain  $S_{xx}$  is written:

$$S_{xx}(z) = (z_0 - z) \frac{d^2 w}{dx^2} = \frac{z - z_0}{\rho} \quad (18)$$

in which  $S_{xx}(z)$  is the  $x$ -directed strain component acting on the face normal to the  $x$ -axis.

The resonator is considered to be isotropic and the stress  $T_i$  can be expressed by the reduced form as follow:

$$T_i = E_i S_{xx} \quad (19)$$

in which  $E_i$  is the Young modulus of the Copper Beryllium. As for the piezoelectric part of the plate, the constitutive relationships among stress, strain and applied field can be expressed in terms of the piezoelectric stress relations

$$\begin{aligned} T_p &= c^E S - e^t \mathcal{E} \\ D &= e S + \epsilon^S \mathcal{E} \end{aligned} \quad (20)$$

in which  $\mathcal{E}$  and  $D$  are respectively the electric field intensity vector and the electric flux density vector.  $c^E$ ,  $e$  and  $\epsilon^S$  are respectively the elastic constants short circuit matrix, the voltage coefficients and dielectric constants matrixes.

Finally, the stress distributions on the  $x$ -faces due to an applied electric field in the  $z$ -direction are:

$$T_{xx}(z) = \begin{cases} E_i S_{xx}(z) & h_p < z < h_p + h_i \\ c_{11p}^E S_{xx} - d_{31} c_{11p}^E \mathcal{E}_z & 0 < z < h_p \end{cases} \quad (21)$$

where  $e^t = d_{31} c_{11p}^E$

Moment balance requires that the moment of forces be zero, as there are no externally applied moments or forces acting on this structure.

$$M = 0 = b \int_z (z - z_0) T_{xx}(z) dz \quad (22)$$

We integrate equation (22) between zero and  $(h_p + h_i)$  (Fig.6) and we use the expressions of  $T_{xx}$  given by (21) and the relation (18).

$$\int_0^{h_p} \frac{(z - z_0)^2}{\rho} c_{11p}^E dz + \int_{h_p}^{h_p + h_i} \frac{(z - z_0)^2}{\rho} E_i dz = \int_0^{h_p} (z - z_0) d_{31} c_{11p}^E \mathcal{E}_z dz = \quad (23)$$

By integrating equation (23), the expression of the curve  $c$  can be deduced:

$$c = \frac{1}{\rho} = \frac{d^2 w}{dx^2} = \frac{3}{2} \frac{d_{31} \mathcal{E}_z}{h_p a} \quad (24)$$

with

$$\frac{1}{a} = \frac{1 - 2f_0}{1 - 3f_0 + 3f_0^2 + \alpha(3\beta + 3\beta^2 + \beta^3 - 6\beta f_0 - 3\beta^2 f_0 + 3\beta f_0^2)} \quad (25)$$

and with

$$\alpha = \frac{E_i}{c_{11p}^E}, \beta = \frac{h_i}{h_p}, f_0 = \frac{z_0}{h_p} \quad (26)$$

By taking into account the boundary conditions of a simply-supported beam and by integrating equation (24) twice, we obtain the displacement profile:

$$w(x) = \frac{3}{4} \frac{d_{31} \mathcal{E}_z}{h_p a} (x^2 - \frac{\lambda}{2} x) \quad (27)$$

and the static deflection at  $\frac{\lambda}{4}$  is given by:

$$\begin{aligned} w_{max} = w\left(\frac{\lambda}{4}\right) &= \frac{-3}{16} \frac{d_{31} \mathcal{E}_z}{h_p} \frac{(\lambda/2)^2}{a} \\ &= -\frac{3}{16} \frac{d_{31} V_z}{h_p^2} \frac{(\lambda/2)^2}{a} \end{aligned} \quad (28)$$

In which  $V_z$  is the voltage applied between the piezo-ceramic electrodes.

2) *Determination of the dynamic deflection:* In order to increase the deflexion, we are going to work at the resonance. That is why in this subsection we have to determine the dynamic deflection which is the static deflection times the dynamic amplification factor.

The dynamic amplification factor is the mechanical quality factor  $Q_m$  of the piezoceramic balanced by the ratio of the strain energy of the entire monomorph  $U_{mono}$  to the strain energy of the piezoelectric layer  $U_{piezo}$  [15].

$$Q = Q_m \frac{U_{mono}}{U_{piezo}} \quad (29)$$

The stored elastic energy in the piezoelectric layer is given by

$$U_{piezo} = \frac{\lambda b}{2} \frac{1}{2} \int_z S_{xx} T_{s_{piezo}} dz \quad (30)$$

Substituting in the expression (30) stress and strain, we obtain:

$$\begin{aligned} U_{piezo} &= \frac{\lambda b}{4} \int_0^{h_p} c_{11p}^E S_{xx}^2 dz \\ &= \frac{\lambda b}{4} \int_0^{h_p} c_{11p}^E \left(\frac{z-z_0}{\rho}\right)^2 dz \\ &= \frac{\lambda b c_{11p}^E h_p^3}{12 \rho^2} \left(1 - \frac{3z_0}{h_p} + \frac{z_0^2}{h_p^2}\right) \\ &= \frac{3}{16} \lambda b h_p d_{31}^2 \mathcal{E}_z^2 c_{11p}^E \frac{1-3f_0+3f_0^2}{a^2} \end{aligned} \quad (31)$$

In the same way, the stored elastic energy in the entire monomorph is given by

$$U_{mono} = \frac{\lambda b}{2} \frac{1}{2} \int_z S_{xx} (T_{s_{piezo}} + T_{s_{reson}}) dz \quad (32)$$

Substituting in the expression (32) stress and strain, we obtain:

$$U_{mono} = \frac{\lambda b}{4} \left( \int_0^{h_p} c_{11p}^E S_{xx}^2 dz + \int_{h_p}^{h_p+h_i} E_i S_{xx}^2 dz \right) \quad (33)$$

Now, from (23), we know that:

$$\begin{aligned} &\int_0^{h_p} d_{31} c_{11p}^E \mathcal{E}_z \left(\frac{z-z_0}{\rho}\right) dz = \\ &\int_0^{h_p} c_{11p}^E \left(\frac{z-z_0}{\rho}\right)^2 dz + \int_{h_p}^{h_p+h_i} E_i \left(\frac{z-z_0}{\rho}\right)^2 dz \end{aligned} \quad (34)$$

Thus, by substituting in the expression (33), we obtain

$$\begin{aligned} U_{mono} &= \frac{\lambda b}{4} \int_0^{h_p} d_{31} c_{11p}^E \mathcal{E}_z \left(\frac{z-z_0}{\rho}\right) dz \\ &= \frac{\lambda b}{8 \rho} d_{31} c_{11p}^E h_p^2 \left(1 - \frac{2z_0}{h_p}\right) \\ &= \frac{3}{16} \lambda b h_p d_{31}^2 \mathcal{E}_z^2 c_{11p}^E \frac{1-2f_0}{a} \end{aligned} \quad (35)$$

Finally,

$$Q = Q_m \frac{a(1-2f_0)}{1-3f_0+3f_0^2} \quad (36)$$

and

$$w_{dyn} = w\left(\frac{\lambda}{4}\right) Q = Q_m \frac{-3}{16} \frac{d_{31} V_z}{h_p^2} \left(\frac{\lambda}{2}\right)^2 \left(\frac{1-2f_0}{1-3f_0+3f_0^2}\right) \quad (37)$$

Since the dynamic deflection (or the amplitude of vibration) is expressed as a function of geometrical parameters for a given voltage value, it could be feasible to bring out the half wavelength beam which meets the guidelines of the "squeeze film effect" study.

3) *Condition on the frequency:* The resonance frequency,  $f_n$ , is a function of the plate dimensions and can be expressed by the following equation:

$$f_n = \left(\frac{\pi}{\lambda/2}\right)^2 \sqrt{\frac{G_b}{M_b}} \quad (38)$$

in which  $M_b$  is the total mass per length, expressed as follow:

$$M_b = \rho_p h_p + \rho_i h_i \quad (39)$$

in which  $G_b$  is the flexional rigidity of the monomorph in N.m.  $G_b$  is the sum of the flexional rigidity of both materials where  $z$  here is measured from the neutral axis.

$$G_b = c_{11p}^E b \int_{piezo} z^2 dz + E_i b \int_{substrate} z^2 dz \quad (40)$$

4) *Neutral line ordinate:* To complement our study, we need to find the neutral line ordinate  $z_0$  as a function of geometrical parameters. Since the neutral line is situated where stresses cancel each other out and change of sign, the sum of stresses at both sides of the line gives a null result. Calculation is carried out in a purely elastic working, i.e. with a null electric field. At  $z_0$ , we can write down

$$0 = \int_z S_{xx} (T_{s_{piezo}} + T_{s_{reson}}) dz \quad (41)$$

After developing this expression, we find:

$$z_0 = \frac{h_p(1 + \alpha\beta^2 + 2\alpha\beta)}{2(1 + \alpha\beta)} \quad (42)$$

5) *Results:* We have at our disposal passive materials in copper-beryllium, and a piezoelectric ceramics PZT, referred to as PI-91, marketed by Saint-Gobain Quartz company ( $\alpha$  is set). The characteristics of the material are indicated in TableII. The voltage supply of piezoactive ceramics is set to 15V in order to avoid a dangerous voltage. Moreover, the thickness of the piezoceramic is 1mm, while the thickness of the substrate is set to 2mm (this value has been chosen to guarantee mechanical holding and fabrication considerations) leading to  $\beta = 2$ .

In Fig.8, the evolution of the absolute value of the dynamic deflection according to the half wavelength,  $w_{dyn}$ , is represented, plotted for the thickness ratio  $\beta = 2$ .

Following the guidelines of the previous section (Fig.5), it is implied that we have to design a plate in which the half wavelength is higher than 8.2 mm (Fig.8) for a supply voltage of 15V. The calculation of the frequency is made for  $b = 49$  mm in order to have a sufficient workspace according to ergonomic requirements.

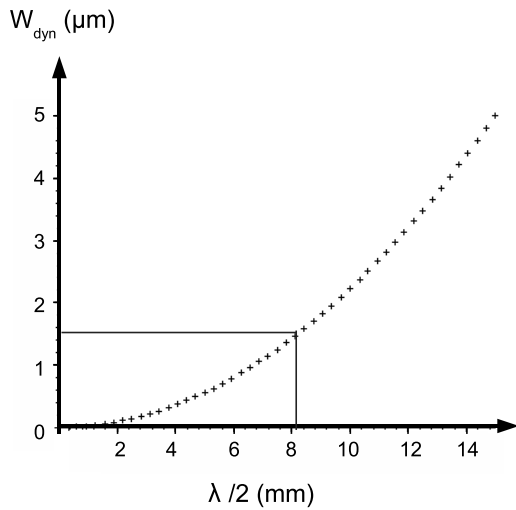


Fig. 8. Dynamic deflection as a function of the half wavelength ( $\lambda/2$ ) for a thickness ratio  $\beta = 2$  and for a supply voltage of 15V.

In Fig.9, the evolution of the resonant frequency obtained from (Eq. 38),  $f_n$ , is represented according to the half wavelength. To match the condition on the frequency according to the squeeze number (Fig. 4), we need  $f_n > 25$ kHz, which implies that the half wavelength needs to be smaller than 14.75 mm.

### C. Numerical study

Now that we know the range of half wavelength required to change the roughness feeling under the fingerpulp for a thickness ratio,  $\beta$ , of 2 and supply voltage of 15V, the final size of the plate remains to be decided. In order to satisfy ergonomic requirements and to check the boundaries of the analytical study (Fig.3), a finite element analysis is performed. The aim of this numerical modeling is to calculate natural frequencies and modal shapes of the plate and to perform harmonic analysis.

TABLE II  
LIST OF PARAMETERS

Mechanical properties of the resonator	
Young modulus $E_i$ ( $10^9 N.m^{-2}$ )	123
Poisson coefficient $\nu_i$	0.31
Mechanical properties of P1-91 ceramic	
Piezoelectric constant $e_{31p}$ ( $C.m^{-2}$ )	-4.9
Elastic constant $c_{11p}^E = \frac{s_{11}^E}{(s_{11}^E)^2 - (s_{12}^E)^2}$ ( $10^{10} N.m^{-2}$ )	6.79
Charge coefficient $d_{31}$ ( $10^{-12} m.V^{-1}$ )	-247
Mechanical quality factor $Q_m$	60
Physical properties of the monomorph structure	
Elastic constant ratio $\alpha$	1.81

1) *Modal analysis considering several half wavelengths:* In this subsection, we calculate the natural frequency of a simply supported beam which length is  $\lambda/2$  and width  $b$  as it is described in the previous section (Fig.6). This analysis is realized using the finite element method (FEM) Ansys software. We consider 7 half wavelengths that measure respectively 9mm, 10mm, 11mm, 12mm, 14mm, 16mm and 20mm. Dimensions and materials used for the simulations are given in TableII and in the Appendix B. The piezoceramics are glued on the mechanical resonator. Numerical results are done for  $b = 49$  mm in order to be compared with the analytical study.

The numerical study (Fig.9) yields to a lower boundary for  $\lambda/2$  (13.6mm) than the one of the analytical study.

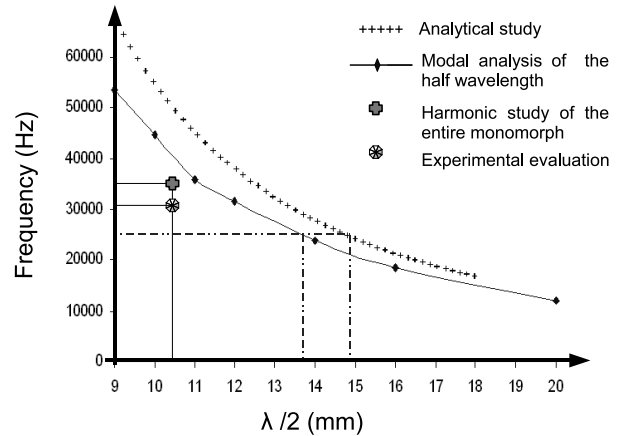


Fig. 9. Natural frequency as a function of the half wavelength: comparison between the analytical and the numerical study.

2) *Choice of the final plate size - modal analysis of the entire monomorph:* We have at our disposal two types of ceramics; the first type measures 15mm and the second type 11mm. Moreover, the dimension of the piezo-ceramics has to approach the size of the half wavelength. And, since the results of the numerical study show that the real frequency is

probably below the predicted frequency, we choose to take the 11mm one in order to take a margin of error. Then, following the requirement for the design, we choose a surface length  $\mathcal{L} = 83\text{mm}$  in order to put 7 ceramics measuring 11mm isolated from each other by a distance of 1mm. The final dimensions of the plate are:  $\mathcal{L} \times b = 83\text{mm} \times 49\text{mm}$ . This gives us a surface area of  $40.67\text{cm}^2$ .

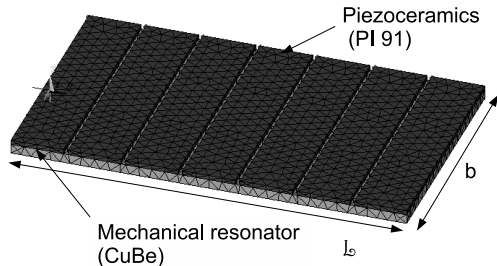


Fig. 10. FE model of the monomorph.

A modal analysis is performed considering the entire monomorph. We find the (8; 0) mode which corresponds to a half-wavelength of  $10.37\text{mm}$  in the X direction. The modal shape is presented in Fig.11 and proves that this resonance frequency (35.6kHz) is in concordance with the squeeze analysis ( $>25\text{kHz}$ ).



Fig. 11. Result of the modal analysis: deformed shape of the (8;0) mode at  $f=35.6\text{kHz}$

3) *Harmonic analysis of the entire monomorph:* We are going to check if those dimensions meet amplitude requirements. The FE model of the monomorph is represented in Figure 10. Those ceramics are activated by two electrical signals, with a  $180^\circ$  phase shift between each. This creates a standing wave.

The harmonic response of the actuator gives the vertical displacement as a function of the frequency (Fig.12) and shows that the natural frequency is located at  $34.77\text{kHz}$ . With this frequency, a vertical displacement of  $3.2\mu\text{m}$  is obtained at the top of the standing wave (cross point reported in Fig.9).

#### IV. EXPERIMENTAL EVALUATION

The prototype is presented in Fig.1. The polarity of each ceramic is oriented to satisfy the wave production along the X direction. The device is supplied by one voltage source adjusted to a mechanical resonance frequency so as to generate

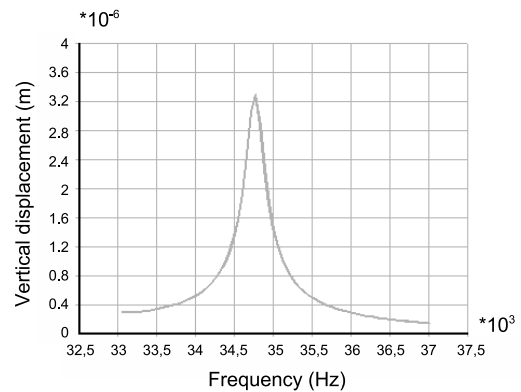


Fig. 12. Result of the harmonic analysis: Vertical displacement of a surface point.

the standing wave along the length of the plate. Some experiments with the prototype built at the laboratory have been performed to confirm analytical and numerical simulations.

#### A. Vibration amplitude measurement

The vibration amplitude is measured using a single-point LASER Doppler Vibrometer (OFV505) linked to a controller (OFV-5000) that is connected to an oscilloscope.

As the results show, a deflection amplitude of about  $2.3\mu\text{m}$  peak to peak is obtained by applying a voltage of 15V. The resonant frequency is  $30.5\text{kHz}$ , (ring point reported on Fig.9) which gives a squeeze number of 15.9 for  $h_r = 0.6\mu\text{m}$ .

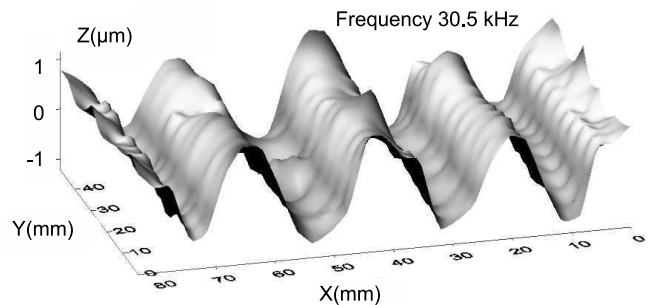


Fig. 13. Laser vibrometric measurements of the (8; 0) mode.

The vibration amplitude of the prototype is smaller than the predicted amplitude. This amplitude attenuation may be due to the manufacturing of the monomorph and especially to the gluing phase. More precisely, the gluing phase is crucial for the vibration quality owing to the ideal gluing hypothesis. However, according to the relative friction study, this vibration amplitude of the plate can be enough to feel the difference of perception. This assumption will be checked in the next section.

#### B. Qualitative study of the sensation

In this subsection, we suggest to test qualitatively the sensation brought by the squeeze film phenomenon in our tactile plate. By controlling the amplitude of the ultrasonic vibration, we will show that we can vary the tactile sensation.

The upper surface of the plate is the surface to touch (Fig.1). The experiment is conducted with twelve naive students aged between 18 and 25 years. In all conditions, all volunteers (9 men, 3 women) wear closed headphones (Fig.14). This allows us to mask the audible cues produced by friction between the finger and the texture. The volunteer's task is to insert the hand horizontally into the box and to bring the elbow in front of the opening. Then, he or she has to form a straight line with a backward motion of the index finger to discover the surface (the tactile plate) presented in the rectangular aperture (Fig.14). As the feeling of lubrication is obtained by vibrating

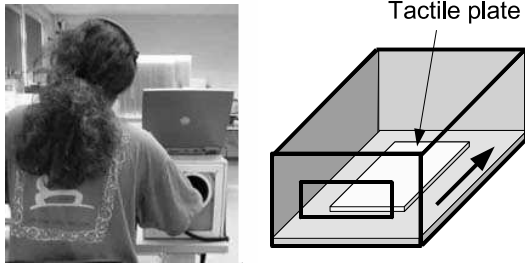


Fig. 14. Experimental setup.

the surface of the plate, we employ 4 virtual surfaces which correspond to 4 amplitudes (peak to peak) of vibration:  $0\mu m$ ,  $0.5\mu m$ ,  $1.2\mu m$  and  $2.3\mu m$ . During the first test, the stimuli are presented when the vibration amplitude decreases. Volunteers are asked to say if there is some differences. If he or she answers "yes", the subject is asked to say what has been removed in this phase. All of the subjects feel clearly the difference during the test, and they immediately say that it is "less slippery".

Finally, a second experience was proposed. Volunteers have to scale their perception with an absolute magnitude estimation as a function of the wave amplitude. For each "virtual surface", the volunteers rate the slipperiness of the surfaces with their own scale after having explored it. The virtual surfaces are always chosen at random. To control the differences in numerical

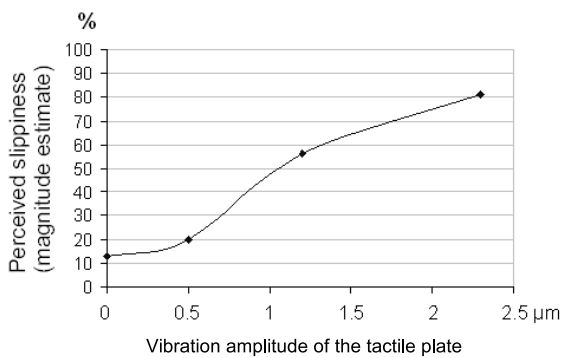


Fig. 15. Mean magnitude estimate as a function of the vibration amplitude of the plate.

scale, the magnitude estimations are multiplied in order to bring back the magnitudes of the scale to 100. In Figure 15, means for the magnitude estimates are shown as a function of the vibration amplitudes of the plate. It also confirms

a variation of the friction coefficient as a function of the vibration amplitude.

## V. CONCLUSION

This work presents theoretical consideration in the design of the ultrasonic tactile plate and verification with experimental results. This design first relies on the squeeze film effect study, which considers the overpressure between a vibrating plate and a fingertip with its epidermal ridges. This helps to deduce some guidelines in term of the vibration amplitude and the average roughness of the plate needed to induce a slippery feeling. In order to generate vibration in the plate and to meet ergonomic requirements, piezoelectric ceramics are glued on a resonator (substrate) made of Copper Beryllium. According to the results of the first study, an analytical study is realized to determine the dynamic deflexion of the beam as a function of geometrical parameters. Results allow us to choose the thickness of the plate and the half-wavelength required to have the vibration amplitude found in the squeeze film study for a given voltage. Then, a numerical study is carried out to calculate the natural frequency and modal shapes of the plate and to check the vibration amplitude stipulated in the analytical study. Experimental trials have been carried out to check performances of the tactile plate. The vibration amplitude is measured and the slippery feeling is qualitatively checked by means of psycho-physic tests. Although this plate is not yet providing different types of texture because the control is not achieved, this allows us to imagine the same results as those found with the control strategy previously studied [4]. Future work should indeed produce different kinds of texture by mean of amplitude modulation.

## APPENDIX A

### RESOLUTION OF THE DIFFERENTIAL EQUATION

$$\frac{1}{2}[1 + \delta \cos(kX)] \frac{d\Psi_{\infty}^2}{dX} + \Psi_{\infty}^2 k \delta \sin(kX) = K \quad (43)$$

$$\frac{d\Psi_{\infty}^2}{\Psi_{\infty}^2} = -2 \frac{\delta k \sin(kX)}{1 + \delta \cos(kX)} dX \quad (44)$$

$$\Psi_1^2 = K_1(X)[1 + \delta \cos(kX)]^2 \quad (45)$$

$$K_1'(X) = \frac{2K}{[1 + \delta \cos(kX)]^3} \quad (46)$$

Since the function  $\Psi_{\infty}^2$  is a square function, it is necessarily an even function, as  $\Psi_{\infty}^2(X) = \Psi_{\infty}^2(-X)$  and  $\frac{d\Psi_{\infty}^2(X)}{dX} = -\frac{d\Psi_{\infty}^2(-X)}{dX}$ . By replacing X by -X in (43), we obtain:

$$\frac{1}{2}[1 + \delta \cos(kX)] \frac{d\Psi_{\infty}^2}{dX} + \Psi_{\infty}^2 k \delta \sin(kX) = -K \quad (47)$$

which implied that  $K = 0$  and that  $K_1'(X) = 0$  from (7).

## APPENDIX B

Material data of Copper-Beryllium :

Density:

$$\rho_i = 8250 \text{ kg.m}^{-3}$$

Material data of the used PZT ceramic PI-91  $11 \times 9 \times 1 \text{ mm}^3$  from Saint-Gobain Quartz company, France.

Density:

$$\rho_p = 7410 \text{ kg.m}^{-3}$$

Stiffness matrix [ $10^{10} \text{ N.m}^{-2}$ ] :

$$c^E = \begin{pmatrix} 12.09 & 7.63 & 7.31 & 0 & 0 & 0 \\ & 12.09 & 7.31 & 0 & 0 & 0 \\ & & 11.26 & 0 & 0 & 0 \\ & & & 3.36 & 0 & 0 \\ & & & & 3.36 & 0 \\ & & & & & 2.23 \end{pmatrix}$$

Piezoelectric constants [ $\text{C.m}^{-2}$ ]:

$$e = \begin{pmatrix} 0 & 0 & 0 & 0 & 17.1 & 0 \\ 0 & 0 & 0 & 0 & 17.1 & 0 \\ -4.9 & -4.9 & 21.4 & 0 & 0 & 0 \end{pmatrix}$$

## ACKNOWLEDGMENT

This work has been carried out within the framework of the INRIA Alcove project and is supported by the IRCICA (Institut de Recherche sur les Composants logiciels et matériels pour l'Information et la Communication Avancée) and The European Commission (FEDER).

## REFERENCES

- [1] M. Benali-Khoudja, M. Hafez, J.-M. Alexandre, A. Kheddar, "Tactile interfaces: a state-of-the-art survey," in *35th International Symposium on robotics*, March 2004.
- [2] D. Pawluk, C. P. van Buskirk, J. H. Killebrew, S. Hsiao, K. Johnson, "Control and pattern specification for high density tactile display," *ASME Dynamic Systems and Control Division*, vol. 64, pp. 97–102, Oct. 1998.
- [3] T. Watanabe, S. Fukui, "A method for controlling tactile sensation of surface roughness using ultrasonic vibration," *IEEE Int. Conf. on Robotics and Automation*, pp. 1134–1139, 1995.
- [4] M. Biet, F. Giraud, F. Martinot, B. Semail, "A piezoelectric tactile display using travelling lamb wave," *Proceedings of Eurohaptics*, pp. 567–570, July 2006.
- [5] T. Maeno, K. Kobayashi, N. Yamazaki, "Relationship between the structure of human finger tissue and the location of tactile receptors," *Bulletin of JSME International Journal*, vol. 41.
- [6] E.O.J. Salbu, "Compressible squeeze films and squeeze bearings," *ASME J. Basic Engng*, vol. 86, pp. 355–366, 1964.
- [7] M. Wiesendanger, "Squeeze film air bearings using piezoelectric bending elements," Ph.D. dissertation, EPFL, Switzerland, 2000.
- [8] A. M. Smith, G. Gosselin, B. Houde, "Deployment of fingertip forces in tactile exploration," *Experimental brain research*, vol. 147, pp. 209–218, September 2002.
- [9] M. Biet, L. Boulon, F. Martinot, F. Giraud, B. Semail, "Using an ultrasonic transducer: Evidence for an anisotropic deprivation of frictional cues in microtexture perception," *To appear in IEEE WorldHaptics*, March 2007.
- [10] J. Pasquero, V. Hayward, "Stress: A practical tactile display system with one millimeter spatial resolution and 700 hz refresh rate," *In Eurohaptics Proceeding, Dublin*, 2003.
- [11] S. J. Lederman, R. L. Klatzky, "Hand movements : a window into haptic object recognition," *Cognitive psychology*, vol. 19, pp. 342–368, 1987.
- [12] F. Martinot, "Caractérisation du rôle de la dynamique du toucher dans la perception de textures," Ph.D. dissertation, USTL Lille; France, 2006.
- [13] L. Landau and E. Lifchitz, *Theory of Elasticity, course of theoretical physics*. Butterworth-Heinemann, 1986.
- [14] V. Monturet, B. Nogareda, "Optimal dimensioning of a piezoelectric bimorph actuator," *The European Physical Journal - Applied Physics*, vol. 17, pp. 107–118, 2002.
- [15] Ahid D. Nashif, David I.G. Jones, John P. Henderson, *Vibration Damping*. John Wiley & Sons, New York, 1985.



**Mélisande Biet** was born in France in 1981. She received his B.Sc. degree in electrical engineering from the University of Science and Technologies of Lille in 2004 and she is currently working toward her Ph.D. degree. Her research interests include mechanical vibrations and modeling and control of piezo-electric actuators.



**Frédéric Giraud** was born in France in 1973. He has graduated from Ecole Normale Supérieure de Cachan, France in 1996 and received the B.S. degree in electrical engineering from Paris-XI University, Orsay, France in 1995, the M.S. Degree in electrical engineering in 1997 from the Institut National Polytechnique de Toulouse, Toulouse, France, and the PhD degree from the Lille University, in 2002. He's a member of the electrical engineering and power electronics laboratory of Lille (L2EP) as an Associate Professeur. His research deals with the modeling and the control of standing wave and traveling wave piezo-electric actuators, for positioning and force feedback applications.



**Betty Semail** was born France in 1964. She received her Ph. D degree in 1990 from University of Paris XI, Orsay and habilitation degree in 1997 from the University of science and technologies of Lille. Since 1990 she has been associate professor in Ecole Centrale of Lille and she is now professor in university of Lille 1. She is a member of the electrical engineering and power electronics laboratory of Lille (L2EP) and responsible of the research axis upon control of electrical systems. She has been working on motors and her main field of interest now deals with the modeling and control of piezo-electric actuators, for positioning and force feedback applications.